Title

Accuracy of the time-averaged ponderomotive approximation for laser-plasma accelerator modeling

Journal

Physics of Plasmas, 28(6)

ISSN

1070-664X

Authors

Terzani, D
Benedetti, C
Schroeder, CB
et al.

Publication Date

2021-06-01

DOI

10.1063/5.0050580

Peer reviewed

Accuracy of the Time-Averaged Ponderomotive Approximation for Laser-Plasma Accelerator Modeling

D. Terzani,[1, a)] C. Benedetti,[1] C. B. Schroeder,[1, 2] and E. Esarey[1]
[1)] *Lawrence Berkeley National Laboratory, Berkeley, California 94720, USA*
[2)] *Department of Nuclear Engineering, University of California, Berkeley, California 94720, USA*

(Dated: May 6, 2021)

Reliable modeling of laser-plasma accelerators, where a short and intense laser pulse propagates in an underdense plasma over long distances, is a computationally challenging task. This is due to the great disparity among the scales involved in the modeling, ranging from the micron scale of the laser wavelength to, for instance, the meter scale of the laser-plasma interaction length for a multi-GeV-class laser-plasma accelerator. To reduce such imbalance the time-averaged ponderomotive approximation may be used, where the plasma particle dynamics is analytically averaged over the laser frequency, and only spatio-temporal scales associated with the laser envelope are retained in the calculations, resulting in significant computational savings. In this paper we characterize the accuracy and robustness of the time-averaged ponderomotive approximation for a range of laser parameters of interest for present and future laser-plasma accelerators, and we show that the error introduced by the averaging process is small in all relevant cases.

I. INTRODUCTION

Plasma-based acceleration has attracted significant theoretical and experimental interest over the past few decades owing to the possibility of generating accelerating gradients that are several orders of magnitude larger than that obtainable in conventional radio-frequency-based accelerators, presently limited to $\lesssim$ 100 MV/m due to material breakdown[1]. In a laser-plasma accelerator (LPA), a short and intense laser pulse propagating in an underdense plasma ponderomotively drives a plasma wave (or wakefield). The wakefield has a relativistic phase velocity and the electromagnetic fields associated with it can accelerate and focus a particle beam properly delayed with respect to the laser driver. LPAs have demonstrated the production of quasi-monoenergetic electron bunches in gas jets[2–4], gas cells[5], and in capillaries discharge waveguides[6–8], reaching energies as high as 8 GeV in a 20 cm-long laser-heated capillary[7].

In the context of modeling the complex nonlinear physics involved in the laser-plasma interaction and particle acceleration, simulation codes based on the Particle-In-Cell (PIC) method have been broadly used for decades[9,10]. However, start-to-end modeling, in 3D, of a multi-GeV class LPA is generally a very computationally-challenging task. This is due to the large disparity between the spatio-temporal scales involved in the modeling, ranging from the $\sim \mu$m scale of the laser wavelength, to the total plasma length, which can be up to a meter for a ∼10 GeV-class LPA stage. Significant efforts are underway to develop highly efficient and highly scalable parallel codes that can reduce the computation time by making use of the possibilities offered by modern hardware architectures (e.g., Graphics Processing Units)[11–14]. However, besides software improvements, and in order to make modeling of multi-GeV LPA stages readily available, a reduction of the computational complexity of the problem is required. This can be achieved by means of the adoption of reduced physics models to describe the laser-plasma interaction. Reduced models allow for significant computational speed-up either because of dimensionality reduction (e.g., 2D cylindrical or quasi-3D instead of full 3D Cartesian)[12,15–17] and/or because of approximations in the description of the physics of the system (e.g., use of quasi-static instead of full plasma response[18–20], use of cold fluid plasma description instead of fully kinetic[15–17,21], use of time-averaged ponderomotive approximation instead of full Lorentz force[22–25], performing the simulation in a Lorentz boosted frame neglecting backward propagating waves[14,26,27], etc.). For instance, in the time-averaged ponderomotive approximation (TPA), also known as the laser envelope approximation or ponderomotive guiding center approximation, the equations describing the motion of the electrons in the fields of the laser and the wake are (analytically) averaged over the fast laser oscillations. This approximation is justified by the fact that, generally, the particle quiver motion in the laser pulse does not couple with the plasma dynamics at the scale of the plasma wavelength. Since the averaging removes the need to model the details of electron motion at the scale of the laser wavelength, the imbalance between the physical scales involved in the simulation is reduced, and a coarser computational mesh can be used. For instance, the longitudinal resolution (i.e., along the direction of laser propagation) can be reduced by a factor $\Omega = \omega_0/\omega_p$, where $\omega_0 = ck_0 = 2\pi c/\lambda_0$ is the laser frequency (k_0 is the laser wavenumber, λ_0 is the laser wavelength, c the speed of light in vacuum), and $\omega_p = (4\pi n_0 q_e^2/m)^{1/2}$ is the plasma frequency (n_0 is the background plasma density, q_e and m are the electron charge and mass, respectively). Additionally, if the tem-

[a)] Electronic mail: DTerzani@lbl.gov

poral step scales with the longitudinal resolution (this is typically the case if the spatial and temporal resolution obey a Courant condition) also the temporal resolution can be reduced by a factor Ω. Hence, assuming the number of particles-per-cell is kept constant, the final speed-up is on the order of Ω^2, resulting in several orders of magnitude reduction in the total computational time required. For instance, for a 10 GeV-class LPA stage where $n_0 \sim 10^{17}$ cm^{-3}, and assuming $\lambda_0 \sim 1$ μm, we have $\Omega \sim 100$, yielding a speed-up of 10^4.

Over the years, the TPA has been exploited in many simulation codes[15,16,22–24,28,29], that have successfully been used for the investigation of several aspects of LPA physics[30–35] and the detailed modeling of experimental setups[6–8,36]. Recently, a new fast and efficient explicit solver for the laser envelope equation has been presented and implemented in the codes `ALaDyn`[25] and SMILEI[37].

Despite the interest that the TPA has attracted in the community, as of today no study is available where the accuracy of this approximation is systematically investigated in the whole domain of laser and plasma parameters of interest for present and future LPA experiments. While for quasi-linear or mildly nonlinear regimes the TPA has been shown to be sufficiently accurate and robust[15,21,23,25,28,37], regimes where the laser pulse is very short (i.e., pulse length $\gtrsim \lambda_0$), ultra-intense (i.e., such that $a_0 \gg 1$, where the laser strength parameter a_0 is defined starting from the peak vector potential of the laser, A_0, as $a_0 = q_e A_0/mc^2$) and tightly focused (i.e., transverse laser size $\gtrsim a_0\lambda_0$) have not been sufficiently explored. A detailed study of the dynamics of a single particle interacting with a laser pulse evolved in the ponderomotive approximation has been presented in Ref. 38; however the laser intensities $I_0 \sim 10^{17}\,\mathrm{W/cm^2}$, where the intensity can be obtained from the relation $I_0[\mathrm{W/cm^2}] \simeq 1.37 \times 10^{18} a_0^2/\lambda_0^2[\mu\mathrm{m}]$, and pulse durations considered $T \sim 200\,\mathrm{fs}$ do not comply with the laser parameters for a present day LPA. Here, we focus on intensities $10^{18}\,\mathrm{W/cm^2} \lesssim I_0 \lesssim 10^{20}\,\mathrm{W/cm^2}$ and pulse durations $3\,\mathrm{fs} \lesssim T \lesssim 100\,\mathrm{fs}$. In these regimes it is not possible to determine *a priori* the accuracy of the particle trajectory averaging associated with the TPA model, since no rigorous analytical description is available. However, numerical experiments show that the TPA tends to be remarkably accurate even in these cases. For instance, this is shown in Fig. 1, where we present a comparison between the wake resulting from a standard full PIC (top half of each panel) and from a TPA simulation (bottom half of each panel) obtained in 2D Cartesian geometry for a laser propagating in a plasma with density of $n_0 = 1.4 \times 10^{18}\,\mathrm{cm^{-3}}$ and a laser profile $a(r,z,t) = a_0 \exp(-r^2/w_0^2)\cos^2[\pi(z-ct)/L]\cos[k_0(z-ct)]$, with $a_0 = 10$, $w_0 = 10\,\mu\mathrm{m}$, $T_{\mathrm{FWHM}} = 8\,\mathrm{fs}$, and $\lambda_0 = 0.8\,\mu\mathrm{m}$, where w_0 is the laser waist, i.e., the transverse position where the intensity drops by a factor e^{-2}, and $cT_{\mathrm{FWHM}} = L_{\mathrm{FWHM}} = 2L\arccos\left(2^{-1/4}\right)/\pi$ is the full width at half maximum (FWHM) length of the pulse intensity. Panel (a) shows a two-dimensional map of the longitudinal electric field normalized to the cold wavebreaking limit $E_{WB} = mc\omega_p/q_e$, while panel (b) shows a map of the electron plasma density. The TPA simulation correctly reproduces, at least macroscopically, all the features observed in the PIC case.

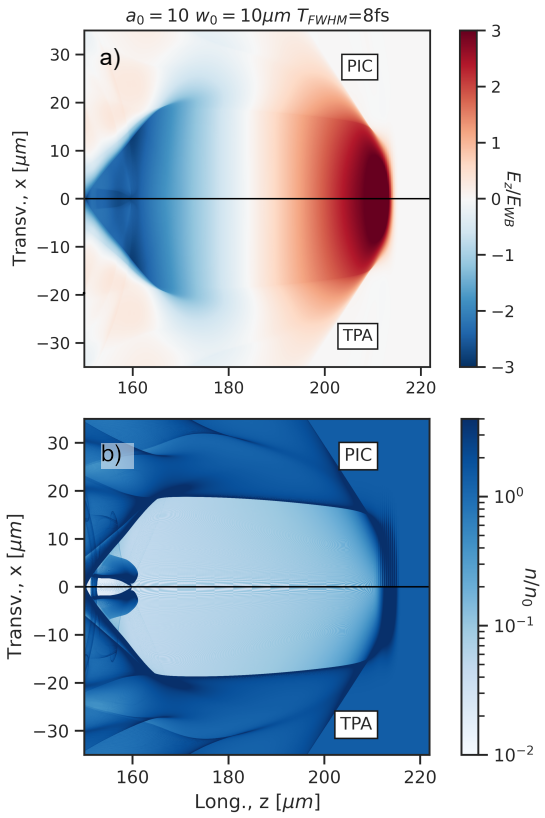

Figure 1. Comparison between a wake obtained with a full PIC (top half of each panel) and in a TPA simulation (bottom half of each panel) in 2D Cartesian geometry for a longitudinally cosine-squared profile and a transversely Gaussian laser driver with $a_0 = 10$, $w_0 = 10\,\mu\mathrm{m}$, $T_{\mathrm{FWHM}} = 8\,\mathrm{fs}$ and $\lambda_0 = 0.8\,\mu\mathrm{m}$ propagating in a uniform plasma with density $n_0 = 1.4 \times 10^{18}\,\mathrm{cm^{-3}}$. Panel (a) shows a two-dimensional map of the longitudinal electric field normalized to the cold wavebreaking limit, panel (b) shows a map of the electron plasma density.

In this paper, we perform a systematic comparison between the results obtained with the non-averaged particle dynamics, computed using, e.g., a standard PIC code, where the particle quiver motion in the laser field is described without approximation, and that using the envelope approximation. We compare the particle phase-space after the interaction with the laser in the two cases quantifying the relative error with a suitable phase-space metric. This allows us to characterize the regimes where the TPA is valid. Additionally, a laser-dependent phenomenological parameter quantifying the quality of the TPA has been identified and correlated with the phase-space error. Studies are performed in vacuum and in plasma assuming a 2D Cartesian geometry. We also pro-

pose an improved expression for the TPA that is more accurate in the case of a tightly focused laser pulse.

The paper is organized as follows. In Sec. II we review the theoretical background of the TPA, showing, by means of a one-dimensional (1D) analysis, how the Hamiltonian is transformed under the two scale separation that characterizes the model and in which limit it tends to the often-quoted Hamiltonian in the ponderomotive approximation. In Sec. III we present a systematic comparison of PIC and TPA simulations, spanning over a broad set of laser parameters (i.e., varying its strength, longitudinal size, and transverse size), exploring regimes of interest for modern and future LPAs, analyzing how the error associated with the TPA affects the single particle dynamics, and investigating how such error affects the wakefield. Conclusions are presented in Sec. IV.

II. THE TIME-AVERAGED PONDEROMOTIVE APPROXIMATION

In order to investigate theoretically the validity of the time-averaged ponderomotive approximation, we consider the motion of a single electron in a laser pulse propagating in the longitudinal, z, direction. Introducing the (longitudinal) co-moving coordinate defined as $\zeta = z - ct$, where t is the time, the dynamics of the system is described by the (normalized) Hamiltonian

$$H\left(\mathbf{x},\mathbf{P}\right) = \sqrt{1+\left|\mathbf{P}+\boldsymbol{a}\right|^2} - P_z, \tag{1}$$

where $\mathbf{x} = (x, y, \zeta)$ denotes the particle coordinates (x and y are the transverse coordinates), $\mathbf{P} = \mathbf{u} - \boldsymbol{a}$ is the normalized (to mc) canonical momentum, $\mathbf{u}$ is the normalized (to mc) particle kinetic momentum, and $\boldsymbol{a} = q_e\mathbf{A}/mc^2$ is the normalized laser vector potential. We note that if the particle interaction time with the laser is much shorter than the laser Rayleigh length, $Z_R = \pi w_0^2/\lambda_0$, i.e., the characteristic length scale for laser evolution, we can treat the laser pulse as non-evolving throughout the interaction, and, hence, the Hamiltonian Eq. (1) is conserved. In this case, and for a particle initially (i.e., before the interaction with the laser) at rest we have that $H = 1$. We consider the (non evolving) laser pulse to be linearly polarized (i.e., $a_y = 0$) and we define its transverse component as

$$a_x = \frac{\hat{a}}{2}e^{ik_0\zeta} + \text{c.c.}, \tag{2}$$

where $\hat{a}$ is the (complex) laser envelope and the exponential term represents the contribution of fast laser oscillations. Under the Coulomb gauge, $\nabla\cdot\boldsymbol{a} = 0$, the longitudinal component of the vector potential is determined by the transverse one according to

$$a_z = \frac{1}{2}\int_\zeta^\infty \partial_x\hat{a}\, e^{ik_0\zeta'}d\zeta' + \text{c.c.}, \tag{3}$$

where we assumed $a_z = 0$ ahead of the laser pulse. In the limit $k_0 L \gg 1$, where L is the characteristic scale length of the laser envelope, the expression above simplifies to

$$a_z \simeq -\frac{1}{2ik_0}\partial_x\hat{a}e^{ik_0\zeta} + \text{c.c.} \tag{4}$$

The Hamiltonian in Eq. (1) can therefore be expanded taking into account the expression in Eq. (4), becoming

$$\left(H+P_z\right)^2 = 1 + \frac{\left|\hat{a}\right|^2}{2} + \left|\mathbf{P}\right|^2 + \frac{\left|\partial_x\hat{a}\right|^2}{2k_0^2} + \frac{\hat{a}^2e^{2ik_0\zeta}+\hat{a}^{*2}e^{-2ik_0\zeta}}{4} + P_x\left(\hat{a}e^{ik_0\zeta}+\hat{a}^*e^{-ik_0\zeta}\right) - \frac{1}{4k_0^2}\left[\left(\partial_x\hat{a}\right)^2e^{2ik_0\zeta} + \left(\partial_x\hat{a}^*\right)^2e^{-2ik_0\zeta}\right] - \frac{2P_z}{k_0}\frac{\partial_x\hat{a}e^{ik_0\zeta} - \partial_x\hat{a}^*e^{-ik_0\zeta}}{2i}. \tag{5}$$

A. 1D case (plane wave laser pulse)

In the 1D limit (i.e., assuming $\partial_x = \partial_y = 0$), and using the conservation of the transverse component of the canonical momentum for a particle in an electromagnetic wave, yielding $P_x = 0$ (i.e., $u_x = a_x$) and $P_y = 0$ (i.e., $u_y = 0$), the Hamiltonian Eq. (5) becomes

$$H_{1D}(\zeta, P_z) = \sqrt{1 + \frac{\left|\hat{a}\right|^2}{2} + P_z^2 + \frac{\hat{a}^2e^{2ik_0\zeta}+\hat{a}^{*2}e^{-2ik_0\zeta}}{4}} - P_z, \tag{6}$$

where $u_z = P_z$ since $a_z = 0$, and the single particle equations of motion are given by Hamilton's equations, $(\dot{\zeta}(t),\, \dot{P}_z(t))^{\mathrm{T}} = (\partial H/\partial P_z,\, -\partial H/\partial\zeta)^{\mathrm{T}}$. Owing to the presence of the rapidly varying term in Eq. (6) (i.e., the terms containing the $e^{\pm 2ik_0\zeta}$ factors), the $(\zeta(t), P_z(t))$ phase-space orbit of a generic particle will contain high-frequency components. For instance, from the constancy of the Hamiltonian Eq. (6) (i.e., $H_{1D} = 1$), we have

$$P_z(\zeta) = u_z(\zeta) = \left|\hat{a}\right|^2/4 + \left(\hat{a}^2e^{2ik_0\zeta} + \hat{a}^{*2}e^{-2ik_0\zeta}\right)/8, \tag{7}$$

where the second term on the right-hand side represents the high frequency component. Averaged phase-space or-

bits, where high-frequency components on the scale of the laser wavelength (or smaller) are smoothed out, can be obtained by introducing the following spatial averaging operator

$$\langle f \rangle (\zeta) = \frac{1}{\lambda_0} \int_{\zeta-\lambda_0/2}^{\zeta+\lambda_0/2} f(\zeta')\, d\zeta', \tag{8}$$

where $f(\zeta)$ is any $\zeta-$dependent function. The averaged momentum (i.e., the momentum of the particle without high-frequency components) is obtained directly by applying the spatial averaging operator to Eq. (7), i.e., $P_{z,av} = \langle P_z \rangle$. Removing the high frequency spatial component in the longitudinal momentum induces a temporal smoothing in the temporal dependence of the particle position. In fact, from Hamilton's equations, $d\zeta/dt = P_z(\zeta)/\gamma(\zeta) - 1$, where, from Eq. (6), $\gamma(\zeta) = 1 + P_z(\zeta)$, and so $[1 + P_z(\zeta)] = -dt/d\zeta$. By applying the spatial operator to the previous equation, we obtain the following expression for the averaged position of the particle, $d\zeta_{av}/dt_{av} = -1/(1 + P_{z,av})$, where t_{av} is a slow time used to parametrize the averaged dynamics. One can show that equations for the averaged phase-space orbit $[\zeta_{av}(t_{av}), P_{z,av}(t_{av})]$ can be obtained from the following Hamiltonian

$$H_{1D,av}(\zeta_{av}, P_{z,av}) \equiv \sqrt{1 + P_{z,av}^2 + \frac{|\hat{a}|^2}{2} + Q} - P_{z,av}, \tag{9}$$

where

$$Q = \left\langle \left[\hat{a}(\zeta)^2 e^{2ik_0\zeta} + \hat{a}^*(\zeta)^2 e^{-2ik_0\zeta}\right]/4 \right\rangle, \tag{10}$$

namely,

$$\left(\dot{\zeta}_{av}(t),\, \dot{P}_{z,av}(t)\right)^T = \left(\frac{\partial H_{1D,av}}{\partial P_{z,av}}, -\frac{\partial H_{1D,av}}{\partial \zeta_{av}}\right)^T. \tag{11}$$

We recall that the 1D TPA Hamiltonian is[1,22,24,39]

$$H_{1D,\mathrm{TPA}}(\zeta_{\mathrm{TPA}}, P_{z,\mathrm{TPA}}) = \sqrt{1 + P_{z,\mathrm{TPA}}^2 + \frac{|\hat{a}|^2}{2}} - P_{z,\mathrm{TPA}}. \tag{12}$$

It is straightforward to verify that in the limit $k_0 L \gg 1$, $Q \to 0$, and so the averaged Hamiltonian $H_{1D,av}$ Eq. (9) reduces to the TPA Hamiltonian $H_{1D,\mathrm{TPA}}$. In practice, already for a pulse length $k_0 L \simeq 4$, corresponding to a FWHM length of ∼1 laser period, the results obtained with the TPA Hamiltonian are essentially indistinguishable from the result obtained with the averaged Hamiltonian, and, hence, both correctly describe the (slow) secular part of the dynamics observed in the exact (non-averaged) case. This is shown in Fig. 2(a), where we plot the evolution of the longitudinal position for a particle interacting with a laser pulse of the form $a_x(\zeta) = a_0 \exp\left(-\zeta^2/L^2\right)\cos(k_0\zeta)$, where $a_0 = 1$, $\lambda_0 = 2\pi/k_0 = 1\,\mu$m, and $k_0 L = 4$.

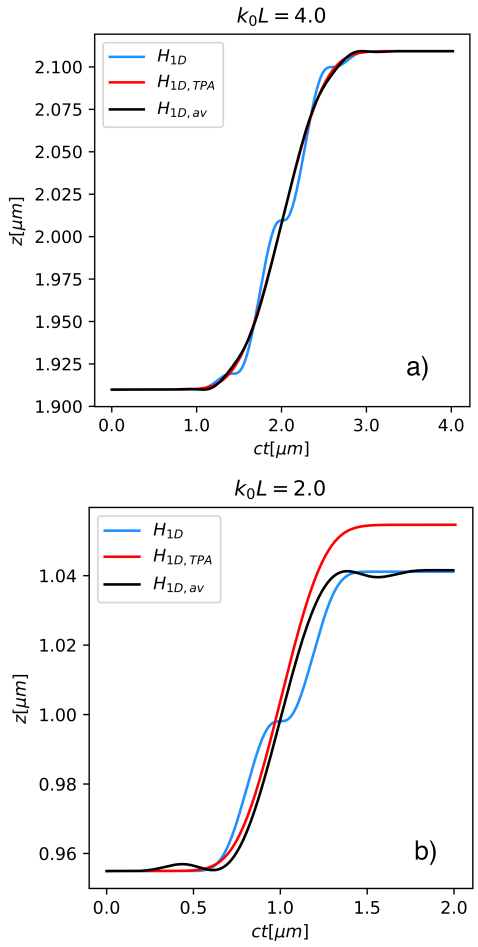

Figure 2. Longitudinal position of a particle interacting with a laser pulse with a Gaussian longitudinal profile and $a_0 = 1$. The blue, red, and black curves are the trajectory obtained using, respectively, the Hamiltonian in Eq. (6), Eq. (12), and Eq. (9). The pulse length is $k_0 L = 4$ in (a), and $k_0 L = 2$ in (b).

The three curves represent the trajectories obtained with the exact Hamiltonian Eq. (6) (blue curve), with the averaged Hamiltonian Eq. (9) (black curve), and with the TPA Hamiltonian Eq. (12) (red curve), respectively. For shorter pulse lengths, as shown in Fig. 2(b), where $k_0 L = 2$ (corresponding to a FWHM length of ∼0.5 laser periods), the TPA trajectory (red curve) deviates from the one obtained with the averaged Hamiltonian (black curve), and it is unable to reproduced the secular dynamics observed in the exact case (blue curve). Note that, in this limit, the particle trajectory is sensitive to the laser phase, also known as carrier envelope phase (CEP). CEP effects in a near single-cycle laser pulse can cause particles interacting with the laser to accumulate a residual transverse momentum that only depends on the phase of the laser pulse[40]. This phase-dependent residual transverse momentum can produce various effects that go beyond a simplified ponderomotive description. We will investigate numerically the implications that CEP effects have

on the validity of the TPA in Sec. III C.

B. 3D case (focused laser pulse)

In the 1D case, the TPA Hamiltonian, formally derived from the exact Hamiltonian, can be heuristically obtained by dropping all the high-frequency terms, and replacing the canonical momentum with its slow (time-averaged) component that describes the secular motion of the particle. Following the same heuristic procedure in the 3D case, starting from Eq. (5), the TPA Hamiltonian reads

$$H_{\text{TPA}} = \sqrt{1 + |\mathbf{P}_{\text{TPA}}|^2 + \frac{|\hat{a}|^2}{2} + \frac{|\partial_x \hat{a}|^2}{2k_0^2}} - P_{z,\text{TPA}}, \quad (13)$$

where $\gamma = (1 + |\hat{a}|^2/2 + |\mathbf{P}_{\text{TPA}}|^2)^{1/2}$, and where $\mathbf{P}_{\text{TPA}}$ denotes the slow (secular) particle momentum without the high-frequency components. The corresponding expression for the ponderomotive force is

$$F_P = -\frac{mc^2}{4\gamma}\nabla\left(|\hat{a}|^2 + \frac{1}{k_0^2}\left|\frac{\partial \hat{a}}{\partial x}\right|^2\right). \quad (14)$$

Note that the expression for the ponderomotive force derived here contains an additional term (i.e., the second term on the right-hand side in Eq. (14)) compared to the expression commonly discussed in the literature[1,38,39,41]. This term, which scales as $\sim 1/(k_0 w_0)^2 = \varepsilon^2$, originates from the longitudinal component of the laser vector potential and it is generally negligible, but may become relevant for tightly focused laser pulses. Previous analytical derivations of the ponderomotive force based on a multiscale expansion of the particle dynamics, e.g. as discussed in Refs. 22, 38, and 39, only considered perturbations to the the quiver motion up to the first order in $\varepsilon \ll 1$ (i.e., a broad laser pulse was assumed). In this limit, corrections to the ponderomotive force arising from the transverse variation of the envelope (e.g., terms of order ε^2) are necessarily neglected.

Due to the non-integrable nature of the dynamics of the system described by Eq. (5), it is not possible to determine *a priori* the error induced in the secular (averaged) dynamics associated with neglecting the high-frequency contributions in Eq. (5). Hence, the accuracy of the TPA needs to be assessed on a case-by-case basis using numerical simulations.

III. NUMERICAL VALIDATION OF TIME-AVERAGED PONDEROMOTIVE APPROXIMATION

In order to systematically investigate the validity of the TPA for the laser parameters of interest for present and future LPA applications, where a clear separation between slow (secular) and fast (motion in the laser field) dynamics might not always be satisfied, we analyzed and compared the motion of a subset of particles interacting with a given laser pulse, either retaining or averaging their motion on the short spatial scales. We performed the tests for a laser pulse propagating in vacuum, where the ponderomotive force is the only force acting on the particles, and in a uniform plasma, where also the effect of the laser-driven plasma wakefield is considered. Modeling for the vacuum case was done by numerically integrating Hamilton's equations for the Hamiltonian Eq. (5) (the laser was assumed to be non-evolving) and the results compared with the ones obtained using the TPA Hamiltonian Eq. (13), with and without the proposed $|\partial_x \hat{a}|^2/k_0^2$ correction. Modeling for the plasma propagation case, where the self-consistent evolution of the laser was taken into account, was done with the PIC code `ALaDyn`[25,42]. Since the dimensionality of the system does not influence the validity of the approximation, all the studies were done in 2D Cartesian geometry.

In the tests, a laser pulse described by the envelope profile

$$\hat{a}(x,\zeta) = a_0 \exp\left(-\frac{x^2}{w_0^2}\right)\cos^2\left(\frac{\pi\zeta}{L}\right), \quad (15)$$

interacts with a sheet (line) of test particles, located at the pulse focal point. Simulations are carried on until all the particles have exited the laser pulse. In all our runs, the laser wavelength was $\lambda_0 = 0.8\,\mu$m. Fig. 3 shows an example of the initial and final phase-space configuration for the test particles for a case with laser pulse parameters $a_0 = 4$, $w_0 = 10\,\mu$m and $T_{\text{FWHM}} = L_{\text{FWHM}}/c = 3\,$fs (vacuum propagation). In Fig. 3, results obtained with the exact dynamics are in black, while TPA results are in red.

In order to quantify the error associated with the TPA, we measure the relative difference between the final particle momenta obtained, respectively, in the non-averaged and TPA cases [see panel (d) in Fig. 3]. An estimate of the error associated with the TPA can be given by the parameter

$$\Delta\widetilde{U} = \left\langle \frac{|\mathbf{u}_P - \mathbf{u}_T|^2}{|\mathbf{u}_P|^2} \right\rangle, \quad (16)$$

where $\mathbf{u}_P$ and $\mathbf{u}_T$ are, respectively, the final particle momenta obtained in the non-averaged and TPA cases, and where the averaging $\langle\cdot\rangle$ represents an ensemble average over the N test particles.

We expect the quality of the TPA approximation, i.e., the value of $\Delta\widetilde{U}$, to be correlated with the following phenomenological parameter

$$\Gamma = a_0^2 \lambda_0^2 \left(\frac{1}{w_0} + \frac{1}{L_{\text{FWHM}}}\right)^2, \quad (17)$$

which represents the variation of the envelope of the laser vector potential over a wavelength both in the longitudinal and in the transverse direction. In fact, one would expect the approximation to fail, i.e., $\Delta\widetilde{U}$ to be large,

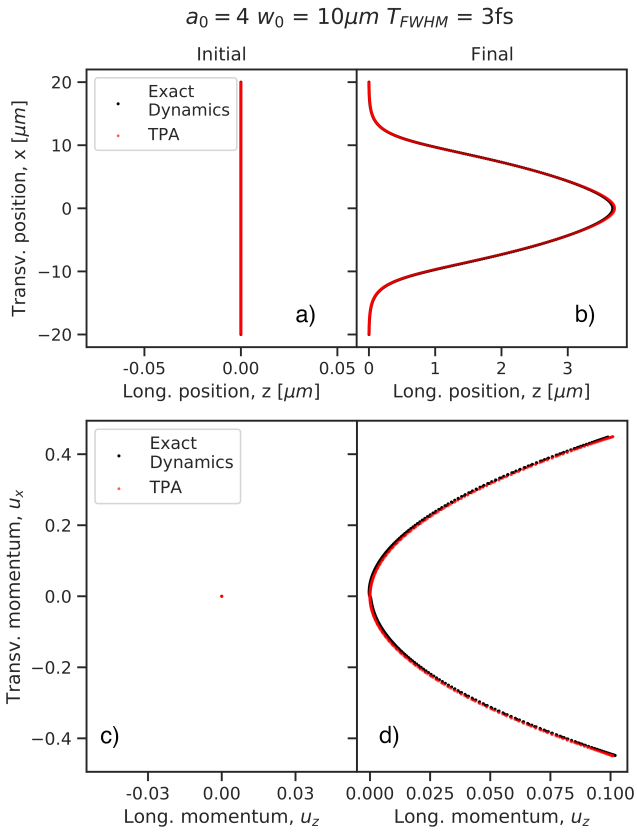

Figure 3. Example of an initial and final test particles configuration after interacting with a laser pulse having $a_0 = 4$, $w_0 = 10\,\mu$m, and $T_{\rm FWHM} = 3\,$fs. Panels (a) and (b) show respectively the initial position and the positions after the end of the interaction with the laser, corresponding to the final time $ct = 6.2\,\mu$m. Panels (c) and (d) show the initial and final time momenta.

Parameter	Values
a_0	0.5, 1, 2, 4, 10
w_0 [μm]	4, 10, 20, 40, 80
$T_{\rm FWHM}$ [fs]	5, 10, 20, 30, 40, 60, 70, 80, 90, 100

Table I. List of laser parameters used for the tests in vacuum.

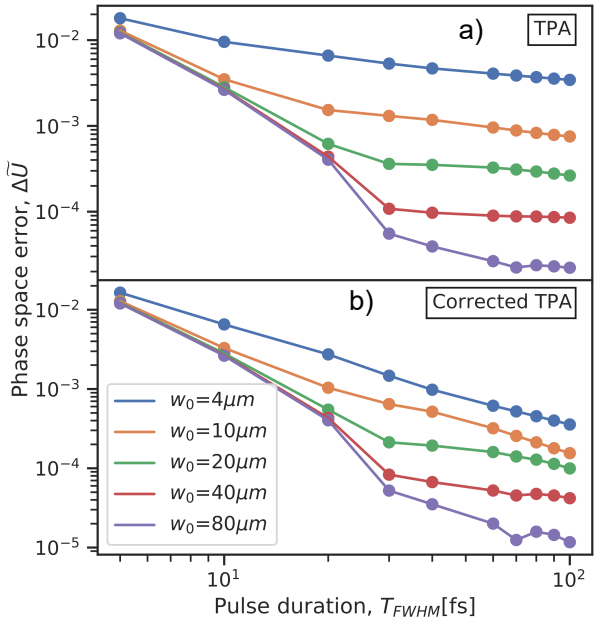

Figure 4. Phase-space error $\Delta\widetilde{U}$ as a function of the FWHM pulse duration $T_{\rm FWHM}$, for different values of w_0 (see figure for details), and for $a_0 = 2$. Results in (a) have been obtained with the conventional expression for the averaged ponderomotive force, the results in (b) have been obtained with the corrected expression Eq. (14).

when Γ is large, i.e., when either the laser pulse is tightly focused, very short, or intense enough that most particles are expelled from the laser region after interacting with the first few laser cycles, invalidating the averaging process required to justify the TPA. On the other hand, when Γ is small, the conditions for the averaging are met (i.e., a generic test particle samples all laser periods during the interaction), and we anticipate $\Delta\widetilde{U}$ to be small.

A. Validation of TPA: test of particle dynamics in vacuum.

For the studies in this section we considered the interaction of the test particles with a non-evolving laser (i.e., a pulse that is rigidly displaced with a constant velocity equal to the speed of light). Hamilton's equations associated with Eqs. (5) and (13) are integrated with a fourth-order Runge-Kutta scheme. Laser parameters were chosen in a broad range of values, shown in Tab. I.

In a first set of tests, we verified if and when the corrected expression for the averaged ponderomotive force proposed in Eq. (14) provides better results than the conventional expression (i.e, the one without the $|\partial_x \hat{a}|^2/k_0^2$ term). Results are shown in Fig. 4, where we plot the phase-space error $\Delta\widetilde{U}$ as a function of the FWHM pulse duration $T_{\rm FWHM}$, for different values of w_0 (see figure for details), and for $a_0 = 2$. Results in (a) have been obtained with the conventional expression for the averaged ponderomotive force, the ones in (b) with the corrected expression Eq. (14). We see that the results obtained with the corrected expression for the pondermotive force are characterized, in general, by a smaller phase-space error. As expected, the effect of the correction is more relevant for tightly focused laser pulses, resulting in a reduction of the error by approximately one order of magnitude for the case $w_0 = 4$ μm (blue curve) in the long pulse limit.

Results for the global comparison between non-averaged and averaged dynamics for all the parameters listed in Tab. I are shown in Fig. 5, where the phase-space error $\Delta\widetilde{U}$ measured at the end of the interac-

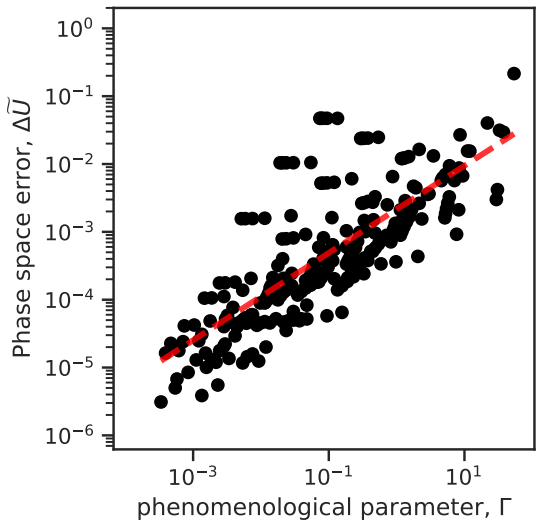

Figure 5. Phase-space error $\Delta\widetilde{U}$ measured at the end of the interaction with the laser as a function of the parameter Γ (every black point represents a given a_0, w_0, and T_{FWHM} combination from Tab. I) for a laser pulse in vacuum. The parameter Γ is a (qualitatively) good predictor of the accuracy of the approximation. The dashed red line represents a guide for the eye.

tion with the laser is plotted as a function of the parameter Γ (every black point represents a given a_0, w_0, and T_{FWHM} combination). The averaged dynamics takes into account the modified version of the ponderomotive force Eq. (14). A (qualitatively) good correlation between $\Delta\widetilde{U}$ and the parameter Γ can be observed. The case with the highest error, $\Delta\widetilde{U} = 2.15 \times 10^{-1}$, occurs for $a_0 = 10$, $w_0 = 4\,\mu$m, and $T_{\text{FWHM}} = 5$ fs (yielding $\Gamma = 53.8$), and indeed corresponds to a ultra-intense, ultra-short, and tightly-focused laser pulse. On the other hand, the lowest error $\Delta\widetilde{U} = 3.11 \times 10^{-6}$ is recorder for $a_0 = 0.5$, $w_0 = 80\,\mu$m, and $T_{\text{FWHM}} = 100$ fs (yielding $\Gamma = 3.36 \times 10^{-4}$) where one would, indeed, expect the averaging to be well justified since a generic particle interacting with the laser will experience several laser periods. Note that for a typical 10 GeV LPA stage operating in the quasilinear regime, one has $a_0 \simeq 1.5$, $w_0 \simeq 70\,\mu$m, and $T_{\text{FWHM}} \simeq 110$ fs, yielding $\Gamma \simeq 3 \times 10^{-3}$. In this case, the error is expected to be $\Delta\widetilde{U} \sim 5 \times 10^{-5}$. Operating in the bubble the parameters are, $a_0 \simeq 4.5$, $w_0 \simeq 40\,\mu$m, and $T_{\text{FWHM}} \simeq 90$ fs, yielding $\Gamma = 5 \times 10^{-2}$, and so $\Delta\widetilde{U} \sim 10^{-4}$. For both cases the use of the TPA to model the laser-plasma interaction seems well justified.

B. Validation of TPA: test of particle dynamics in plasma.

For the studies in this section we considered the TPA in the context of wake excitation. In this case, plasma particles interact with both the self-consistent laser driver and the wakefields. Hence, the final phase-space error $\Delta\widetilde{U}$ is determined not only by the averaging process of fast dynamics in the laser field, but also by the particle dynamics in the wake. Since in this work we are interested in characterizing the validity of the TPA, it is important to record the phase-space of the test particles used to evaluate $\Delta\widetilde{U}$ as early as possible after the end of the interaction with the laser pulse. Also, tracked test particles were chosen sufficiently far from the vacuum-plasma interface in order to mitigate effects related to vacuum-plasma transition, that may produce phase-spaces that are complex to analyze. We would like to point out that the TPA can be used to model density transitions, even in case of sharp gradients[43] (i.e. the length of the transition is comparable with the pulse length), and transitions from vacuum to plasma and viceversa.

Particular care was adopted in order to minimize numerical errors in both the full PIC and TPA simulations. In fact, as we saw in the previous subsection, the TPA provides results that are generally very close to the ones obtained in the non-averaged cases. Hence, minimizing spurious numerical errors is important to correctly isolate the effects of the TPA. In order to establish reliable results, we progressively increased the horizontal and vertical grid resolution and the number of numerical particles per cell until we noticed no significant variation in the final particle distribution. We also verified the convergence of the laser pulse propagation velocity (verifying that is the same in the PIC and TPA cases). We ultimately set a longitudinal cell size of $\Delta z = 0.01\,\mu$m, a transverse cell size $\Delta x = 2\Delta z$, and a temporal integration step $c\Delta t = 0.64\Delta z$ for both the PIC and the TPA simulations. The number of particles per cell was $N_{\text{PPC}} = 12$ in all runs. The need for such a high resolution is due to the slow convergence of full PIC simulations. In fact, scales associated with the laser wavelength need to be resolved well in order to mitigate the dispersive error associated with the Finite Difference Time Domain solver, which introduces errors in the laser pulse group velocity, and to correctly describe the particles trajectories when they are quivering in the electromagnetic field of the laser pulse[44,45]. On the other hand, simulations based on the TPA and on a laser envelope solver are considerably less demanding. Particles do not present oscillations on short scales and the error introduced by the pusher is small, moreover the pulse propagation speed is correctly reproduced already at very low resolutions[25]. For instance, for the laser-plasma parameters considered in this study, TPA simulations were essentially converged for a resolution $\Delta z \simeq 0.05\,\mu$m, resulting in a considerable reduction of the cost of the simulation owing to the smaller mesh dimension, larger time integration step, and smaller total number of particles. However, in this study, setting the same grid and temporal resolution for the full PIC and TPA simulations was necessary in order to obtain easily comparable results in terms of final particle distributions (e.g., output data at the same time in both codes, etc.).

As reported in Ref. 44, in 2D Cartesian geometry us-

Parameter	Values
a_0	2, 4, 10
w_0 [μm]	4, 10, 20
$T_{\rm FWHM}$ [fs]	8, 20, 40, 60

Table II. List of laser parameters used for laser-plasma interaction simulations.

ing a laser with in-plane or out-of-plane polarization produces equivalent effects from the point of view of wake excitation. However, it was also noted that simulations with in-plane polarization are affected by a significantly higher degree of noise, and reaching convergence of the physics requires higher resolutions and more particles-per-cell compared to the out-of-plane case. Hence, for this study all the simulations considered a laser driver with an out-of-plane polarization. Due to the relatively large computational cost of LPA simulations performed with a sufficiently high resolution to keep numerical errors as low as possible, it was not possible to carry out an extensive parameter scan as the one presented in the vacuum case. Hence, we restricted our analysis to a relevant subset of cases, as listed in Tab. II. In all the tests we fixed the background plasma density to the value $n_0 = 1.4 \times 10^{18}\text{cm}^{-3}$, which is the resonant value for a laser pulse with $T_{\rm FWHM} = 20\,\text{fs}$, which is the median of all the values considered in Tab. II.

In all the TPA simulations presented here the modified expression for the ponderomotive force given by Eq. (14) was used. Note that the numerical implementation of the modified expression for the ponderomotive force in simulation codes that are already featuring the standard TPA is straightforward. In fact, it only requires the interpolation of the gradient of the vector potential from the computational grid, where the laser envelope is known, to the particle position. A Boris-like particle pusher as the one described in Ref. 25 can then be used. The computational overhead from the inclusion of the additional term in the evaluation of the ponderomotive force is negligible. However, contrary to what was observed in the previous subsection with tests in vacuum, we noticed that the introduction of the modified expression for the ponderomotive force does not significantly affect the simulation results (i.e., the phase-space errors, $\Delta\widetilde{U}$, measured in the cases of the standard and modified expression for the averaged ponderomotive force are essentially equal). We believe this is due to the higher numerical noise that characterizes fully self-consistent laser-plasma simulations. This noise, not present in the case of simple test-particle simulations, masks any improvement associated with the modified expression for the ponderomotive force. However, we were not able to verify this hypothesis by further increasing the resolution or the number of particles per cell in our runs due to the high computational time required.

Results for the global comparison between non-averaged and averaged dynamics for all the parameters listed in Tab. II are shown in Fig. 6, where we plot the

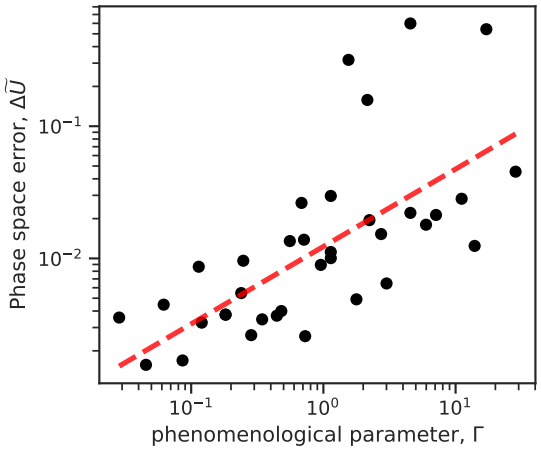

Figure 6. Scatter plot of $\Delta\widetilde{U}$ in function of Γ regarding the interaction of a laser pulse with a uniform plasma. As for the interaction in vacuum, Γ is related to the accuracy of the approximation and can be used for an *a-priori* estimate of it. The red dashed line represents a guide for the eye.

phase-space error $\Delta\widetilde{U}$ as a function of the phenomenological parameter Γ for a laser pulse propagating in a uniform plasma. We notice that, similarly to what was observed in the previous subsection, there is a qualitatively good correlation between Γ and $\Delta\widetilde{U}$, but the typical $\Delta\widetilde{U}$ in this case is about an order of magnitude larger than in the corresponding case in vacuum. Here, the highest error, $\Delta\widetilde{U} = 0.62$, occurs for $\Gamma = 17.1$, and in particular for the laser parameters $a_0 = 10$, $w_0 = 10\,\mu\text{m}$, and $T_{\rm FWHM} = 8\,\text{fs}$, which correspond to the highest intensity and shortest pulse duration among all the tested values. The large error in this case can be ascribed to the particles close to the center of the laser pulse. Such particles undergo a strongly nonlinear interaction, i.e., both their longitudinal and transverse momentum are u_x, $u_z \gg 1$ before exiting the pulse, and the averaged dynamics cannot correctly describe the motion[22]. When considering the propagation in a plasma, the conditions for a typical 10 GeV LPA stage operating in the bubble regime, i.e. $a_0 \simeq 4.5$, $w_0 \simeq 40\,\mu\text{m}$, $T_{\rm FWHM} \simeq 90\,\text{fs}$, and therefore $\Gamma \simeq 5 \times 10^{-2}$, correspond to $\Delta\widetilde{U} \lesssim 10^{-3}$.

C. Effect of the TPA-induced phase-space error on global wakefield properties

In this section we analyze how the phase-space error in the particle distribution associated with the TPA affects the macroscopic (i.e., integrated) properties of the wakefield.

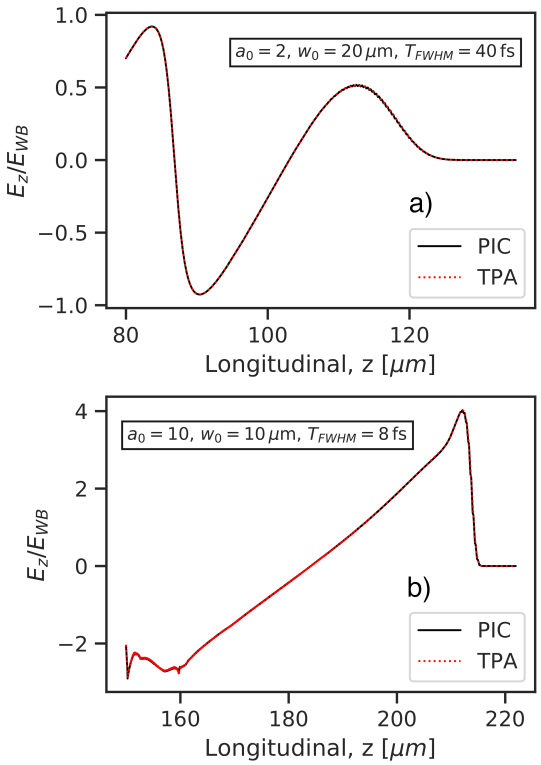

Figure 7. On-axis longitudinal lineout of the accelerating field, E_z/E_{WB}, obtained in a full PIC simulation (solid black line) and in a TPA simulation (dotted red line) for a set of parameters corresponding to the smallest (a) and the largest (b) phase-space error $\Delta\widetilde{U}$ shown in Fig. 6.

1. Effect on the longitudinal wakefield

In Fig. 7 we compare the on-axis longitudinal wakefield, E_z/E_{WB}, obtained in a full PIC simulation (solid black line) and in a TPA simulation (dotted red line) for a set of parameters corresponding to the smallest [Fig. 7(a)] and the largest [Fig. 7(b)] phase-space error $\Delta\widetilde{U}$ shown in Fig. 6. As it can be seen, even in the case of the largest error, results obtained with the TPA reproduce very closely the unaveraged PIC results. In order to perform a more quantitative analysis of the role of the TPA-induced phase-space error, we consider the slope of the longitudinal wakefield at the phase location corresponding to its first zero crossing behind the driver, i.e., $m = \partial_\zeta E_z|_{\zeta=\zeta_0}$, where ζ_0 is such that $E_z(\zeta_0) = 0$. A precise comparison of this quantity measured in the full PIC and TPA cases is meaningful if the laser is short enough that its field components vanish or are negligible for $\zeta = \zeta_0$. Note that, as opposed to, for instance, other wake-related quantities such as the maximum value of the accelerating wakefield, this quantity is well defined and easy to measure in simulations even in strongly nonlinear regimes. In Fig. 8 we show, as an example, the evaluation of m, represented by the slope of the red dashed line, in a

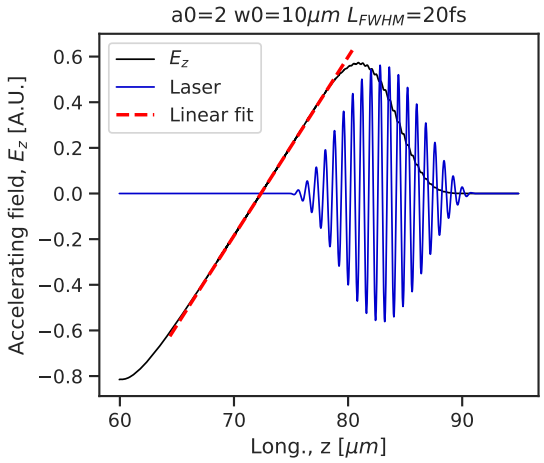

Figure 8. Evaluation of m, represented by the slope of the red dashed line, in a full PIC simulation with parameters $a_0 = 2$, $w_0 = 10\,\mu$m and $T_{\rm FWHM} = 20$ fs. At the point where $E_z = 0$, i.e. $z \simeq 72\,\mu$m, the laser pulse electric field is negligible, therefore the slope can be compared to the corresponding one measured in the TPA, where laser oscillations are absent.

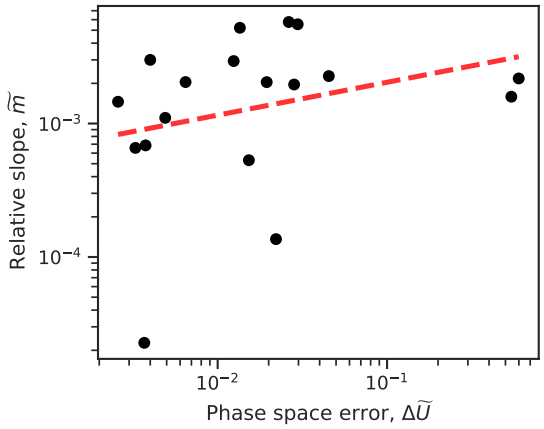

Figure 9. Normalized difference between the slopes of the longitudinal wakefields in the full PIC and TPA wakefields, $\widetilde{m}$, measured for the available cases, i.e., when $T_{\rm FWHM} \leq 20$ fs, plotted as function of $\Delta\widetilde{U}$. The red dashed line serves as a guide for the eye.

full PIC simulation with parameters $a_0 = 2$, $w_0 = 10\,\mu$m, and $T_{\rm FWHM} = 20$ fs. We defined the normalized difference between the slopes of the longitudinal wakefields in the full PIC and TPA wakefields as $\widetilde{m} = (m_P - m_T)/m_P$, where m_P and m_T are the values of the slope of E_z at the zero crossing of the field in the full PIC and TPA cases, respectively. We have only been able to measure $\widetilde{m}$ for pulses having $T_{\rm FWHM} \leq 20$ fs since longer lasers overlap with the zero-crossing point. In Fig. 9 we show $\widetilde{m}$ measured for the available cases plotted as function of $\Delta\widetilde{U}$. As it can be seen, the relative difference between the slopes of E_z in a full PIC and in a TPA is always

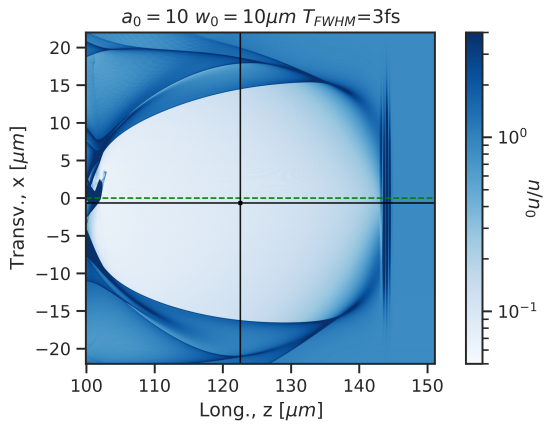

Figure 10. Colormap of the plasma density excited by a laser pulse having $a_0 = 10$, $w_0 = 10\,\mu$m and $T_{\rm FWHM} = 3$ fs, propagating in a uniform plasma of density $n_0 = 3.5\times10^{18}$ cm^{-3} for $ct = 100\,\mu$m. The green dashed line indicates the laser symmetry axis. The two black solid lines identify respectively the longitudinal and transverse position of the wakefield centroid $(z_0,\, x_0) \simeq (122\,\mu\text{m},\, -1\,\mu\text{m})$.

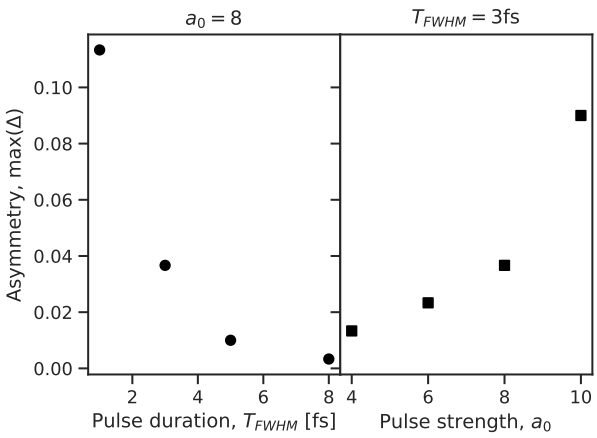

Figure 11. On the left, wakefield maximum asymmetry measured in function of the laser duration for fixed $w_0 = 10\,\mu$m and $a_0 = 8$. On the right, same plot for fixed $w_0 = 10\,\mu$m and $T_{\rm FWHM} = 3$ fs in function of the laser strength.

$\widetilde{m} < 10^{-2}$. We also note that the correlation between $\widetilde{m}$ and $\Delta\widetilde{U}$, although observable, is weak.

2. Effect on the symmetry of the wakefield.

It is well known that for an ultra-short and ultra-intense laser pulse CEP effects play an important role in the dynamics. As shown in Refs. 40 and 46, for a strongly relativistic interaction, a multi-scale expansion in terms of the vector potential $\boldsymbol{a}(\mathbf{x}, t)$ of the equation of motion of a particle interacting with the laser field shows that the third order terms of the solution depend on the fast laser oscillations (note that the second order terms corresponds to the ponderomotive force, which, as we know, does not depend on the laser oscillations). In particular, the third order momentum dependence from the laser fast oscillating phase has an amplitude such that $\delta u_x^{(3)} \sim 1/(k_0 L_{\rm FWHM})^2$, so it becomes relevant for a short (i.e, almost single-cycle) laser pulse, where particles acquire a momentum in the direction of the laser polarization that depends on the laser phase. Such momentum perturbation is even with respect to the particle initial transverse position r_0, i.e., $\delta u_x^{(3)}(x = r_0) = \delta u_x^{(3)}(x = -r_0)$. This will result in an asymmetry in the transverse structure of the wakefield that cannot be described in the framework of the TPA. Understanding the breakdown point of the averaged ponderomotive approximation is therefore important when dealing with ultra-short lasers.

We define the transverse wake asymmetry as $\Delta = x_0/w_0$, where x_0 is the transverse position of the wake centroid, defined as the location of the zero crossing of the transverse wakefield, i.e., the location where $E_x(x_0, \zeta_0) - B_y(x_0, \zeta_0) = 0$ (E_x and B_y are the transverse electric and magnetic field components in the wake, respectively). The longitudinal position where x_0 is measured is $\zeta = \zeta_0$, corresponding to the zero crossing of the longitudinal wakefield in the first plasma period behind the driver. We emphasize that our goal is to define an accuracy threshold under which the approximation is considered valid, therefore our set of laser and plasma parameters are chosen so that the maximum asymmetry is reached within the first Rayleigh length, where the laser pulse evolution is negligible. In Fig. 10 we show the plasma density obtained from the propagation of a laser having $a_0 = 10$, $w_0 = 10\,\mu$m, and $T_{\rm FWHM} = 3$ fs in a uniform plasma of density $n_0 = 3.5\times10^{18}$ cm^{-3} after $ct = 100\,\mu$m of propagation. The green dashed line indicates the symmetry axis of the laser pulse. The wakefield centroid is in $(z_0,\, x_0) \simeq (122\,\mu\text{m},\, -1\,\mu\text{m})$, and the black solid lines highlight its coordinates. The centroid transverse position is not on axis due to the CEP effects (we note that in a purely TPA description the centroid is always on axis) and the injected bunch presents some transverse oscillations.

Simulation results for the maximum wake asymmetry reached in the first 300 μm of propagation (corresponding to about one Rayleigh length) are shown in Fig. 11. For these simulations the laser has a waist $w_0 = 10\,\mu$m and propagates in a uniform plasma with density $n_0 = 3.5 \times 10^{18}$ cm^{-3}. Results for a fixed laser strength, $a_0 = 8$, as a function of the pulse duration are shown in Fig. 11 (a). We see that the asymmetry increases when reducing the pulse duration. Results for a fixed pulse duration, $T_{\rm FWHM} = 3$ fs, and different laser intensities are shown in Fig. 11 (b). As expected, the asymmetry grows with the laser intensity.

By defining a maximum level of wake asymmetry, Δ_{max}, for which the TPA approximation is still considered acceptable, we can use the results presented in

Fig. 11 to constrain the corresponding laser parameters. For instance, by selecting $\Delta_{max} = 0.05$, we have that the corresponding wake asymmetry will be below 5% as long as we have $T_{\text{FWHM}} \gtrsim 3\,\text{fs}$ and $a_0 \lesssim 8$. Note that, however, the laser driver needs to satisfy these requirements at any time in a TPA simulation run. In fact, when performing the modeling of a realistic LPA stage, even though the initial laser parameters might be acceptable from the point of view of TPA modeling, nonlinear laser evolution (i.e., laser self-steepening and laser depletion/redshifting[47,48]) might cause the depleted laser to enter a regime where then use of TPA might not be justified anymore. It is worth noticing that the asymmetry induced by the CEP effects also influences the particles dynamics in the wakefield. In this case, a TPA description of the system can therefore result in an inaccurate evolution of a trapped and accelerating particle beam, particularly if generated by self-injection as pointed out in Ref. 40.

IV. CONCLUSIONS

In this paper we analyzed and characterized the accuracy of the TPA for a range of laser parameters of interest for present and future LPA applications.

In the TPA, the equations describing the motion of an electron interacting with the laser pulse and the wake are analytically averaged over the fast laser oscillations, and so electron dynamics on the scale of the laser wavelength need not be modeled. This results in a reduction of the computational complexity associated with the modeling of the laser-plasma interaction in an LPA, allowing for considerable computational speedups.

In this work, we performed a systematic comparison between the particle dynamics obtained in the case of the exact, non-averaged, dynamics computed using a standard PIC code or a dedicated test particle code, and that using the TPA. We compared the particle phase-space after the interaction with the laser in the two cases quantifying the relative error with a suitable phase-space metric. This phase-space error was correlated with a laser-dependent phenomenological parameter quantifying the quality of the TPA. Studies were performed in vacuum and in plasma. We also proposed and tested an improved expression for the TPA valid in the case of a tightly focused laser pulse.

We have shown that in a broad range of laser parameters, namely $T_{\text{FWHM}} \gtrsim 3\,\text{fs}$, $w_0 \gtrsim 4\,\mu\text{m}$ and $a_0 \lesssim 10$ (a laser wavelength of $0.8\,\mu\text{m}$ was assumed), the TPA describes the system very accurately, and we quantified this accuracy for the first time. For instance, for a 10 GeV LPA stage operating in the nonlinear regime and driven by a laser pulse with parameters $a_0 \simeq 4.5$, $w_0 \simeq 40\,\mu\text{m}$, and $T_{\text{FWHM}} \simeq 90\,\text{fs}$, the phase-space error associated with the TPA is $\Delta\widetilde{U} \lesssim 10^{-3}$. The TPA introduces relatively low errors even in extreme cases, such as for a laser having $a_0 = 10$, $w_0 = 4\mu\text{m}$, and $T_{\text{FWHM}} = 8\,\text{fs}$. The phase-space error in this case is $\Delta\widetilde{U} \sim 10^{-1}$, and so the TPA can be used to reliably describe such regimes.

Tests in vacuum showed that the improved expression for the ponderomotive force provided here produced more accurate results than the conventional expression in the case of tightly-focused laser pulses, namely for $w_0 \lesssim 10\,\mu\text{m}$. However, no measurable improvements were observed for the tests in plasma. We believe this is due to the higher numerical noise that characterizes fully self-consistent laser-plasma simulations.

Lastly, the role that the phase-space error associated with the TPA has on the integrated wake properties, such as the structure of the longitudinal wakefield and the symmetry of the wake, was also investigated. In particular, we found that for laser parameters typically employed in a GeV-class LPA stage, namely $T_{\text{FWHM}} \gtrsim 10\,\text{fs}$, $a_0 \lesssim 10$ and $w_0 \gtrsim 10\,\mu\text{m}$, the wakefield properties are retrieved effectively by the TPA and the differences with respect to the results obtained with a full PIC simulation are unimportant. CEP effects can introduce a significant asymmetry in the wakefield in case of ultra-intense ($a_0 \sim 10$) and almost single-cycle ($T_{\text{FWHM}} \sim 3\,\text{fs}$) laser pulses. We characterized the level of asymmetry for a fixed laser waist $w_0 = 10\,\mu\text{m}$ and we found that as long as the duration and the strength are respectively $T_{\text{FWHM}} \gtrsim 3\,\text{fs}$ and $a_0 \lesssim 8$, it remains below 5% and the effects on the plasma dynamics are negligible.

The choice of laser wavelength used in this study $\lambda_0 = 0.8\,\mu\text{m}$, was motivated by the fact that Ti:Sa is currently the most widespread high-power laser technology used as driver in today's LPA experiments. Of course, TPA can be used with other wavelengths provided that the ratio between the laser wavelength and the characteristic size (transverse and longitudinal) of the laser envelope is small enough in such way that a multiscale expansion of the dynamics holds.

ACKNOWLEDGMENTS

This work was supported by the Director, Office of Science, Office of High Energy Physics, of the U.S. Department of Energy under Contract No. DE-AC02-05CH11231, and used the computational facilities at the National Energy Research Scientific Computing Center (NERSC). The authors wish to thank C.G.R. Geddes for the insightful discussions.

The data that support the findings of this study are available from the corresponding author upon reasonable request.

REFERENCES

[1]E. Esarey, C. Schroeder, and W. Leemans, "Physics of laser-driven plasma-based electron accelerators," Reviews of Modern Physics **81**, 1229 (2009).

[2]J. Faure, Y. Glinec, A. Pukhov, S. Kiselev, S. Gordienko, E. Lefebvre, J.-P. Rousseau, F. Burgy, and V. Malka, "A laser–

plasma accelerator producing monoenergetic electron beams," Nature **431**, 541 (2004).
[3]S. P. Mangles, C. Murphy, Z. Najmudin, A. G. R. Thomas, J. Collier, A. E. Dangor, E. Divall, P. Foster, J. Gallacher, C. Hooker, *et al.*, "Monoenergetic beams of relativistic electrons from intense laser–plasma interactions," Nature **431**, 535–538 (2004).
[4]C. Geddes, C. Toth, J. Van Tilborg, E. Esarey, C. Schroeder, D. Bruhwiler, C. Nieter, J. Cary, and W. Leemans, "High-quality electron beams from a laser wakefield accelerator using plasma-channel guiding," Nature **431**, 538–541 (2004).
[5]X. Wang, R. Zgadzaj, N. Fazel, Z. Li, S. Yi, X. Zhang, W. Henderson, Y.-Y. Chang, R. Korzekwa, H.-E. Tsai, *et al.*, "Quasi-monoenergetic laser-plasma acceleration of electrons to 2 gev," Nature communications **4**, 1–9 (2013).
[6]W. Leemans, A. Gonsalves, H.-S. Mao, K. Nakamura, C. Benedetti, C. Schroeder, C. Tóth, J. Daniels, D. Mittelberger, S. Bulanov, *et al.*, "Multi-gev electron beams from capillary-discharge-guided subpetawatt laser pulses in the self-trapping regime," Physical review letters **113**, 245002 (2014).
[7]A. Gonsalves, K. Nakamura, J. Daniels, C. Benedetti, C. Pieronek, T. de Raadt, S. Steinke, J. Bin, S. Bulanov, J. van Tilborg, *et al.*, "Petawatt laser guiding and electron beam acceleration to 8 gev in a laser-heated capillary discharge waveguide," Physical review letters **122**, 084801 (2019).
[8]A. Gonsalves, K. Nakamura, C. Benedetti, C. Pieronek, S. Steinke, J. Bin, S. Bulanov, J. van Tilborg, C. Geddes, C. Schroeder, *et al.*, "Laser-heated capillary discharge plasma waveguides for electron acceleration to 8 gev," Physics of Plasmas **27**, 053102 (2020).
[9]C. K. Birdsall and A. B. Langdon, *Plasma physics via computer simulation* (CRC press, 2004).
[10]R. W. Hockney and J. W. Eastwood, *Computer simulation using particles* (crc Press, 1988).
[11]F. Rossi, P. Londrillo, A. Sgattoni, S. Sinigardi, and G. Turchetti, "Towards robust algorithms for current deposition and dynamic load-balancing in a gpu particle in cell code," in *AIP Conference Proceedings*, Vol. 1507 (American Institute of Physics, 2012) pp. 184–192.
[12]R. Lehe, M. Kirchen, I. A. Andriyash, B. B. Godfrey, and J.-L. Vay, "A spectral, quasi-cylindrical and dispersion-free particle-in-cell algorithm," Computer Physics Communications **203**, 66–82 (2016).
[13]M. Bussmann, H. Burau, T. E. Cowan, A. Debus, A. Huebl, G. Juckeland, T. Kluge, W. E. Nagel, R. Pausch, F. Schmitt, U. Schramm, J. Schuchart, and R. Widera, "Radiative signatures of the relativistic kelvin-helmholtz instability," in *Proceedings of the International Conference on High Performance Computing, Networking, Storage and Analysis*, SC '13 (ACM, New York, NY, USA, 2013) pp. 5:1–5:12.
[14]J.-L. Vay, A. Almgren, J. Bell, L. Ge, D. Grote, M. Hogan, O. Kononenko, R. Lehe, A. Myers, C. Ng, *et al.*, "Warp-x: A new exascale computing platform for beam–plasma simulations," Nuclear Instruments and Methods in Physics Research Section A: Accelerators, Spectrometers, Detectors and Associated Equipment **909**, 476–479 (2018).
[15]C. Benedetti, C. Schroeder, E. Esarey, C. Geddes, and W. Leemans, "Efficient modeling of laser-plasma accelerators with inf&rno," in *AIP Conference Proceedings*, Vol. 1299 (AIP, 2010) pp. 250–255.
[16]P. Tomassini and A. Rossi, "Matching strategies for a plasma booster," Plasma Physics and Controlled Fusion **58**, 034001 (2015).
[17]A. Marocchino, F. Massimo, A. Rossi, E. Chiadroni, and M. Ferrario, "Efficient modeling of plasma wakefield acceleration in quasi-non-linear-regimes with the hybrid code architect," Nuclear Instruments and Methods in Physics Research Section A: Accelerators, Spectrometers, Detectors and Associated Equipment **829**, 386–391 (2016).
[18]P. Tomassini, A. Giulietti, D. Giulietti, and L. Gizzi, "Thomson backscattering x-rays from ultra-relativistic electron bunches and temporally shaped laser pulses," Applied Physics B **80**, 419–436 (2005).
[19]C. Huang, V. K. Decyk, C. Ren, M. Zhou, W. Lu, W. B. Mori, J. H. Cooley, T. M. Antonsen Jr, and T. Katsouleas, "Quickpic: A highly efficient particle-in-cell code for modeling wakefield acceleration in plasmas," Journal of Computational Physics **217**, 658–679 (2006).
[20]T. Mehrling, C. Benedetti, C. Schroeder, and J. Osterhoff, "Hipace: a quasi-static particle-in-cell code," Plasma physics and controlled fusion **56**, 084012 (2014).
[21]D. Terzani, P. Londrillo, P. Tomassini, and L. Gizzi, "Numerical implementation of a hybrid pic-fluid framework in laser-envelope approximation," in *Journal of Physics: Conference Series*, Vol. 1596 (IOP Publishing, 2020) p. 012062.
[22]P. Mora and T. M. Antonsen, Jr, "Kinetic modeling of intense, short laser pulses propagating in tenuous plasmas," Physics of Plasmas **4**, 217–229 (1997).
[23]D. Gordon, W. Mori, and T. Antonsen, "A ponderomotive guiding center pic code for modeling laser-plasma accelerations," in *APS Division of Plasma Physics Meeting Abstracts* (1999).
[24]B. Cowan, D. Bruhwiler, E. Cormier-Michel, E. Esarey, C. Geddes, P. Messmer, and K. Paul, "Characteristics of an envelope model for laser–plasma accelerator simulation," Journal of Computational Physics **230**, 61–86 (2011).
[25]D. Terzani and P. Londrillo, "A fast and accurate numerical implementation of the envelope model for laser–plasma dynamics," Computer Physics Communications **242**, 49–59 (2019).
[26]J.-L. Vay, "Noninvariance of space-and time-scale ranges under a lorentz transformation and the implications for the study of relativistic interactions," Physical review letters **98**, 130405 (2007).
[27]M. Kirchen, R. Lehe, S. Jalas, O. Shapoval, J.-L. Vay, and A. R. Maier, "Scalable spectral solver in galilean coordinates for eliminating the numerical cherenkov instability in particle-in-cell simulations of streaming plasmas," Physical Review E **102**, 013202 (2020).
[28]P. Messmer and D. L. Bruhwiler, "Simulating laser pulse propagation and low-frequency wave emission in capillary plasma channel systems with a ponderomotive guiding center model," Phys. Rev. ST Accel. Beams **9**, 031302 (2006).
[29]D. F. Gordon, "Improved ponderomotive guiding center algorithm," IEEE transactions on plasma science **35**, 1486–1488 (2007).
[30]C. Benedetti, C. Schroeder, E. Esarey, F. Rossi, and W. Leemans, "Numerical investigation of electron self-injection in the nonlinear bubble regime," Physics of Plasmas **20**, 103108 (2013).
[31]S. Shiraishi, C. Benedetti, A. Gonsalves, K. Nakamura, B. Shaw, T. Sokollik, J. van Tilborg, C. Geddes, C. Schroeder, C. Tóth, *et al.*, "Laser red shifting based characterization of wakefield excitation in a laser-plasma accelerator," Physics of Plasmas **20**, 063103 (2013).
[32]W. Zhu, J. Palastro, and T. Antonsen, "Pulsed mid-infrared radiation from spectral broadening in laser wakefield simulations," Physics of Plasmas **20**, 073103 (2013).
[33]P. Tomassini, S. De Nicola, L. Labate, P. Londrillo, R. Fedele, D. Terzani, and L. Gizzi, "The resonant multi-pulse ionization injection," Physics of Plasmas **24**, 103120 (2017).
[34]P. Tomassini, D. Terzani, F. Baffigi, F. Brandi, L. Fulgentini, P. Koester, L. Labate, D. Palla, and L. Gizzi, "High-quality 5 gev electron bunches with resonant multi-pulse ionization injection," Plasma Physics and Controlled Fusion **62**, 014010 (2019).
[35]P. Tomassini, D. Terzani, L. Labate, G. Toci, A. Chance, P. Nghiem, and L. Gizzi, "High quality electron bunches for a multistage gev accelerator with resonant multipulse ionization injection," Physical Review Accelerators and Beams **22**, 111302 (2019).
[36]S. Steinke, J. Van Tilborg, C. Benedetti, C. Geddes, C. Schroeder, J. Daniels, K. Swanson, A. Gonsalves, K. Nakamura, N. Matlis, *et al.*, "Multistage coupling of independent laser-plasma accelerators," Nature **530**, 190–193 (2016).

[37]F. Massimo, A. Beck, J. Dérouillat, M. Grech, M. Lobet, F. Pérez, I. Zemzemi, and A. Specka, "Efficient start-to-end 3d envelope modeling for two-stage laser wakefield acceleration experiments," Plasma Physics and Controlled Fusion **61**, 124001 (2019).
[38]B. Quesnel and P. Mora, "Theory and simulation of the interaction of ultraintense laser pulses with electrons in vacuum," Physical Review E **58**, 3719 (1998).
[39]E. Startsev and C. McKinstrie, "Multiple scale derivation of the relativistic ponderomotive force," Physical Review E **55**, 7527 (1997).
[40]E. Nerush and I. Y. Kostyukov, "Carrier-envelope phase effects in plasma-based electron acceleration with few-cycle laser pulses," Physical review letters **103**, 035001 (2009).
[41]P. Mora and T. M. Antonsen Jr, "Electron cavitation and acceleration in the wake of an ultraintense, self-focused laser pulse," Physical Review E **53**, R2068 (1996).
[42]C. Benedetti, A. Sgattoni, G. Turchetti, and P. Londrillo, "`ALaDyn`: A high-accuracy pic code for the maxwell–vlasov equations," IEEE Transactions on plasma science **36**, 1790–1798 (2008).
[43]T. Silva, A. Helm, J. Vieira, R. Fonseca, and L. Silva, "On the use of the envelope model for down-ramp injection in laser-plasma accelerators," Plasma Physics and Controlled Fusion **62**, 024001 (2019).
[44]E. Cormier-Michel, B. A. Shadwick, C. G. R. Geddes, E. Esarey, C. B. Schroeder, and W. P. Leemans, "Unphysical kinetic effects in particle-in-cell modeling of laser wakefield accelerators," Physical Review E **78**, 016404 (2008).
[45]A. V. Arefiev, G. E. Cochran, D. W. Schumacher, A. P. Robinson, and G. Chen, "Temporal resolution criterion for correctly simulating relativistic electron motion in a high-intensity laser field," Physics of Plasmas **22**, 013103 (2015).
[46]J. Huijts, I. Andriyash, L. Rovige, A. Vernier, and J. Faure, "Carrier-envelope phase effects in laser wakefield acceleration with near-single-cycle pulses," arXiv preprint arXiv:2006.10566 (2020).
[47]C. B. Schroeder, C. Benedetti, E. Esarey, and W. Leemans, "Nonlinear pulse propagation and phase velocity of laser-driven plasma waves," Physical review letters **106**, 135002 (2011).
[48]C. Benedetti, F. Rossi, C. Schroeder, E. Esarey, and W. Leemans, "Pulse evolution and plasma-wave phase velocity in channel-guided laser-plasma accelerators," Physical Review E **92**, 023109 (2015).